Int. J. Heat Mass Transfer. Vol. 17, pp. 197–204. Pergamon Press 1974. Printed in Great Britain

HYPERSONIC RADIATING MERGED SHOCK LAYER NEAR THE BLUNT-BODY STAGNATION REGION*

AJAY KUMAR and A. C. JAIN†
Department of Aeronautical Engineering, Indian Institute of Technology, Kanpur. India

(*Received* 27 *February* 1973 *and in revised form* 30 *July* 1973)

Abstract—In the low Reynolds number flow, shock wave and viscous layer near the stagnation point of a blunt-body are merged together. This merged shock layer is investigated in this paper for a radiating gas. The radiating transfer is simplified to the emission-dominated case. The basic model of the flow is described by the full Navier–Stokes equations. Using the concept of local similarity, the equations are reduced to an eighth-order set of nonlinear, coupled ordinary differential equations. This set of equations is integrated numerically from the surface to the freestream under different prescribed conditions. Earlier, this problem was investigated by Liu and Sogame [3] within the framework of two thin-layer model. A number of inaccuracies of this analytical development are pointed out. It is shown that the present analysis gives more reliable and accurate information about the detailed behaviour of the radiating viscous flow at low Reynolds number.

NOMENCLATURE

c_H, heat transfer coefficient, $\bar{q}_w/\bar{\rho}_\infty \bar{u}_\infty(\bar{H}_\infty - \bar{H}_w)$;
c_p, specific heat at constant pressure;
$\bar{H}$, total enthalpy;
h, dimensionless enthalpy, $\bar{h}/\bar{u}_\infty^2$;
$\bar{k}$, coefficient of heat conductivity;
M_∞, freestream Mach number;
p, dimensionless pressure, $\bar{p}/\bar{\rho}_\infty \bar{u}_\infty^2$;
Pr, Prandtl number;
$\bar{Q}$, radiative energy loss per unit mass;
$\bar{q}_w$, rate of energy transferred to body surface;
$\bar{q}_w^R$, radiative energy flux to body surface;
R, gas constant;
r, dimensionless radial distance, $\bar{r}/\bar{r}_b$;
$\bar{r}_b$, body radius;
Re, Reynolds number, $\bar{\rho}_\infty \bar{u}_\infty \bar{r}_b/\bar{\mu}_0$;
T, temperature, $\bar{T}/\bar{T}_0$;
u, dimensionless tangential velocity component, $\bar{u}/\bar{u}_\infty$;
$\bar{u}_\infty$, freestream velocity;
v, dimensionless normal velocity component, $\bar{v}/\bar{v}_\infty$;
α, absorption coefficient;
Γ, ratio of radiative energy emission to energy convection;
γ, ratio of specific heats;
η, transformed radial coordinated;
θ, angle between r and axis of symmetry;
κ, mass absorption coefficient;
μ, dimensionless viscosity coefficient, $\bar{\mu}/\bar{\mu}_0$;
ρ, dimensionless density, $\bar{\rho}/\bar{\rho}_\infty$;
σ, Stephan–Boltzman constant.

Superscript
$\bar{}$, dimensional quantities.

Subscripts
w, wall conditions;
∞, freestream conditions;
0, stagnation conditions.

1. INTRODUCTION

WHEN a space vehicle re-enters the earth atmosphere, the temperature of the gas is very high and thermal radiation becomes an important mode of heat transfer. A complete analysis of such high temperature flow field should be based upon a study of interaction between a moving gas and a radiation field. Radiation decreases the total energy of the shock layer gas and it is often referred to as the radiation cooling effect. This radiation cooling has significant effect on the velocity and temperature profiles in the shock layer. It also reduces the convective heat transfer to the surface.

At low Reynolds number, a thick shock wave merges with the adjoining viscous zone near the stagnation region of a blunt-body and it is difficult to distinguish between the two. This is generally called 'Merged Shock Layer'. A detailed review of the pertinent literature for a perfect gas is given by Cheng [1] and Jain [2]. Liu and Sogame [3] in their paper investigated the effect of radiation cooling in the merged shock layer within the framework of two thin-

* This work was supported by the Ministry of Defence, Govt. of India, under a Grant-in-Aid Project entitled 'Hypersonic Flow at Low Reynolds Numbers'.

† Presently on leave at Marshall Space Flight Center, Huntsville, Ala., U.S.A.

layer model of Cheng [4, 5]. The model basically consists of a thin shock wave followed by a thin viscous layer. The usual Rankine–Hugonoit relations are modified by the presence of transport and radiative effects behind the shock wave. For the sake of simplicity, they considered the emission-dominated case in which the radiative heat flux due to emission is much larger than due to reabsorption. The gas ahead of the shock structure was assumed cold and neither absorbing nor emitting. By an iterative technique, they solved the problem of shock layer and shock wave like zones separately.

Recently, Adimurthy and Jain [6] considered in detail the basic model of the flow, that may possibly exist near the stagnation region in the low Reynolds number regime, within the framework of Navier–Stokes equations and compared the results with Cheng's analysis and other available theoretical and experimental data. They found that the thin-layer approximation can not adequately describe the detailed structure of the flow in the low Reynolds number regime. It is to be expected as Cheng investigated the viscous zone by neglecting the pressure variation across it which seems to be appreciable from the present analysis. The thickness of the merged shock layer is also of the order of body radius making the thin-layer approximation invalid at low Reynolds numbers. Moreover, in the two thin-layer model of Cheng, there lies a discontinuity in the temperature at the interface of the shock wave and the shock layer and the flow does not merge smoothly with the free-stream.

For reasons stated above, modification of Cheng's analysis by the introduction of radiation effects will lead to inaccurate results at low Reynolds number. In the present investigation, we have considered the radiation cooling effects on the detailed structure and heat transfer characteristics of the flow. The flow is described by the full Navier–Stokes equations. The energy equation is modified by introducing the radiative term. Using the concept of local similarity, the above equations are reduced to an eighth-order set of nonlinear, coupled ordinary differential equations which are integrated by a successive accelerated replacement technique from the surface to the free-stream. It is found that with our formulation, there is no discontinuity in any of the flow quantity and the flow quantities merge smoothly with the freestream. In the present investigation, the temperature level in the merged shock layer is slightly higher, the merged shock layer is thicker, the decrease in the thickness due to radiation cooling is smaller and the radiative heat transfer coefficient is higher than in Liu and Sogame's [3] work. We could also obtain the pressure variation in the merged shock layer. Above $Re = 25$, the various flow profiles in the merged shock layer are very close to that of two thin-layer model.

Finally, we may add that most of the earlier work on radiating shock layer near the stagnation region of a blunt-body is valid only for high Reynolds number. Howe and Viegas [7] introduced radiation effects in the viscous layer model. Burggraf [8] used the method of asymptotic expansions for large Reynolds numbers considering only the emission-dominated case. Hoshizaki and Wilson [9] obtained the solutiions of a viscous radiating shock layer using an integral method. In [10], they further introduced the effects of self-absorption and mass injection also.

2. GOVERNING EQUATIONS OF MOTION

In this paper, the assumption of a perfect gas having constant specific heat and a linear viscosity law is made. The radiative transfer term is simplified to the emission-dominated case. This is valid when the smallest local photon mean freepath is large compared to the thickness of the merged shock layer. The gas is assumed to be gray with a frequency-averaged absorption coefficient which depends on the local pressure and temperature. The effects of radiation on the pressure and internal energy of the gas are neglected since the temperature is not so high as to make these effects considerable. The cold wall case is considered.

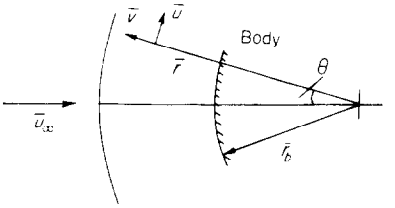

FIG. 1a. Dimensional coordinate system.

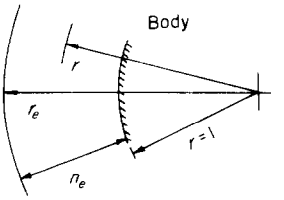

FIG. 1b. Dimensionless coordinate system.

In the coordinate system defined in Fig. 1, the basic nondimensional form of the equations of motion on an axisymmetric body are

$$r(\rho v)_r + (\rho u)_\theta + \rho(2v + u\cot\theta) = 0 \tag{1}$$

$$\frac{p_\theta}{r} + \rho\left(vu_r + \frac{u}{r}u_\theta + \frac{uv}{r}\right) = \frac{1}{r^2 Re}\left[\frac{4\mu}{3}(u_\theta + v) - \frac{2\mu}{3}(rv_r + v + u\cot\theta)\right]_\theta + \frac{1}{Re}\left[\mu r\left(\frac{u}{r}\right)_r + \frac{\mu}{r}v_\theta\right]_r + \frac{3\mu}{rRe}\left[r\left(\frac{u}{r}\right)_r + \frac{v_\theta}{r}\right] + \frac{2\mu\cot\theta}{r^2 Re}[u_\theta - u\cot\theta] \tag{2}$$

$$p_r + \rho\left(vv_r + \frac{u}{r}v_\theta - \frac{u^2}{r}\right) = \frac{1}{Re}\left[\frac{4u}{3}v_r - \frac{2\mu}{3r}(u_\theta + 2v + u\cot\theta)\right]_r + \frac{1}{rRe}\left[\mu r\left(\frac{u}{r}\right)_r + \frac{\mu}{r}v_\theta\right]_\theta + \frac{4\mu}{rRe}\left(v_r - \frac{v}{r}\right) - \frac{\mu}{r^2 Re}\left[2u_\theta + 2u\cot\theta - r^2\left(\frac{u}{r}\right)_r\cot\theta - v_\theta\cot\theta\right] \tag{3}$$

$$\rho\left(vh_r + \frac{u}{r}h_\theta\right) = vp_r + \frac{u}{r}p_\theta + \frac{\mu}{Re}\left[2v_r^2 + \frac{2}{r^2}(u_\theta + v)^2 + \frac{2}{r^2}(v + u\cot\theta)^2 + \left\{r\left(\frac{u}{r}\right)_r + \frac{v_\theta}{r}\right\}^2\right] - \frac{2\mu}{3r^2 Re}[rv_r + u_\theta + 2v + u\cot\theta]^2 + \frac{1}{r\,Pr\,Re}\left[\left(\frac{\mu}{r}h_\theta\right)_\theta + (\mu r h_r)_r + \mu\left(h_r + \frac{\cot\theta}{r}h_\theta\right)\right] - \rho Q \tag{4}$$

$$p = (\gamma - 1)\rho h/\gamma \tag{5}$$

$$\mu = T \tag{6}$$

where subscripts denote partial differentiation.

In the above equations, variables are nondimensionalized as

$$v = \bar{v}/\bar{u}_\infty,\ u = \bar{u}/\bar{u}_\infty,\ \rho = \bar{\rho}/\bar{\rho}_\infty,\ T = \bar{T}/\bar{T}_0,\ \mu = \bar{\mu}/\bar{\mu}_0,$$
$$h = \bar{h}/\bar{u}_\infty^2,\ r = \bar{r}/\bar{r}_b,\ Pr = c_p\bar{\mu}/\bar{k},\ Re = \bar{\rho}_\infty\bar{u}_\infty\bar{r}_b/\bar{\mu}_0$$

where $\bar{\mu}_0$ is the viscosity coefficient at freestream stagnation temperature $\bar{T}_0$.

Boundary conditions are

(i) On the body

$$u = v = 0,\ h = h_w$$

(ii) In the freestream

$$u = \sin\theta,\ v = -\cos\theta,\ \rho = 1,\ h = 1/(\gamma - 1)M_\infty^2.$$

In equation (4), $-\rho Q$ represents the radiative heat loss and is given by

$$\rho Q = (4\bar{\rho}\kappa\sigma\bar{T}^4)/(\bar{\rho}_\infty\bar{u}_\infty^3/\bar{r}_b). \tag{7}$$

The gray volumetric absorption coefficient $\bar{\rho}\kappa$ is assumed to be of the form taken by Traugott [11]

$$\alpha = \bar{\rho}\kappa = C\bar{p}\bar{T}^4$$

where C is a constant.

Substituting α in equation (7), it can be shown that

$$\rho Q = (\Gamma_0\alpha_0\bar{r}_b)\,ApT^8 \tag{8}$$

where

$$\Gamma_0 = \frac{4\sigma\bar{T}_0^4}{\bar{\rho}_\infty\bar{u}_\infty c_p\bar{T}_0},\ \alpha_0 = C(\bar{\rho}_\infty\bar{u}_\infty^2)\,\bar{T}_0^4$$

and

$$A = \frac{c_p\bar{T}_0}{\bar{u}_\infty^2} = \frac{1}{2} + \frac{1}{(\gamma - 1)M_\infty^2}.$$

We assume the following form of the solution about the axis of symmetry

$$\begin{aligned} u(r,\theta) &= u_1(r)\sin\theta \\ v(r,\theta) &= v_1(r)\cos\theta \\ \rho(r,\theta) &= \rho_1(r) \\ h(r,\theta) &= h_1(r) \\ p(r,\theta) &= p_1(r) + p_2(r)\sin^2\theta \\ \mu(r,\theta) &= \mu_1(r) \end{aligned} \tag{9}$$

where the terms with subscripts 1 and 2 are functions of r only. Let

$$\frac{r - 1}{r_e - 1} = \eta \text{ and } r_e - 1 = n_e \text{ so that } r = 1 + n_e\eta.$$

Here, r_e and n_e define the location of the freestream from the origin and from the body respectively as shown in Fig. 1b.

Substituting (9) in equations (1)–(6) and changing the independent variable r to η, we obtain

$$\frac{\rho_1'}{\rho_1} = \frac{n_e}{(1 + n_e\eta)v_1}\left[-2(u_1 + v_1) - \left(\frac{1 + n_e\eta}{n_e}\right)v_1'\right] \tag{10}$$

$$\frac{u_1''}{n_e^2} = \left(\frac{u_1 + v_1}{1 + n_e\eta}\right)\left[\frac{8}{3(1 + n_e\eta)} + \frac{\mu_1'}{n_e\mu_1} + \frac{Re\rho_1 u_1}{\mu_1}\right]$$

$$+\frac{v_1'}{3n_e(1+n_e\eta)}+Re\left[\frac{\rho_1 v_1 u_1'}{n_e\mu_1}+\frac{2p_2}{\mu_1(1+n_e\eta)}\right]-\frac{u_1'}{n_e}\left[\frac{2}{(1+n_e\eta)}+\frac{\mu_1'}{n_e\mu_1}\right] \quad (11)$$

$$\frac{v_1''}{n_e^2}=\frac{3}{4}\frac{Re}{\mu_1 n_e}(p_1'+\rho_1 v_1 v_1')-\frac{v_1'}{n_e}\left[\frac{\mu_1'}{n_e\mu_1}+\frac{2}{(1+n_e\eta)}\right]-\frac{u_1'}{2n_e(1+n_e\eta)}+\left(\frac{u_1+v_1}{1+n_e\eta}\right)\left[\frac{\mu_1'}{n_e\mu_1}+\frac{7}{2(1+n_e\eta)}\right] \quad (12)$$

$$\frac{p_2'}{n_e}=-\frac{p_1'}{n_e}+\rho_1 u_1\left(\frac{u_1+v_1}{1+n_e\eta}\right) \quad (13)$$

$$\frac{A\rho_1 v_1 T_1'}{n_e}(1+n_e\eta)^2=(1+n_e\eta)^2\left[\frac{v_1 p_1'}{n_e}+\frac{2\mu_1 v_1'^2}{n_e^2 Re}\right]-\frac{2\mu_1}{3Re}\left[\frac{(1+n_e\eta)v_1'}{n_e}+2(u_1+v_1)\right]^2+\frac{4\mu_1}{Re}(u_1+v_1)^2+\frac{A(1+n_e\eta)}{Re\,Pr\,n_e}\left[2\mu_1 T_1'+\frac{(1+n_e\eta)}{n_e}(\mu_1' T_1'+\mu_1 T_1'')\right]$$

$$-(1+n_e\eta)^2(\Gamma_0\alpha_0\bar{r}_b)Ap_1T_1^8 \quad (14)$$

$$p_1=(\gamma-1)\rho_1 h_1/\gamma \quad (15)$$

$$\mu_1=T_1. \quad (16)$$

Here, a prime denotes differentiation with respect to η.

The boundary conditions become

(i) On the body ($\eta = 0$)

$$u_1=v_1=0,\ T_1=T_w=T_\infty \text{ or } T_1=T_w=0{\cdot}1$$

(ii) In the freestream ($\eta = 1$)

$$u_1=1,\ v_1=-1,\ \rho_1=1,$$

$$T_1=\left[1+\frac{\gamma-1}{2}M_\infty^2\right]^{-1},\quad p_2=0.$$

3. METHOD OF SOLUTION

Equations (10)–(16) constitute a set of nonlinear, coupled ordinary differential equations with split boundary conditions. These equations are integrated by a finite-difference method known as Successive Accelerated Replacement (SAR) method. The method is successfully used earlier by Dellinger [12] and by Adimurthy and Jain [6]. There are two salient features of this method. One is that it involves the application of one particular equation only for the correction of one particular unknown variable in each iteration. The second is that the corrections applied to the values of the variables at each of the mesh points are controlled by "acceleration factors' which prevent the iteration scheme from diverging. Thus, a successful application of this method does not critically depend on how well the initial guesses approximate the converged solution. SAR method is applied only for the second-order equations, while the first-order equations are solved by direct numerical quadrature. There are three differential equations of second-order which may be written as

$$U(u_1'', u_1', v_1', \mu_1', u_1, v_1, \mu_1, \rho_1, p_2, n_e)=0 \quad (17)$$

$$V(v_1'', v_1', u_1', p_1', \mu_1', u_1, v_1, \mu_1, \rho_1, n_e)=0 \quad (18)$$

$$T(T_1'', T_1', v_1', \mu_1', p_1', u_1, v_1, \mu_1, \rho_1, p_1, T_1, n_e)=0 \quad (19)$$

where prime denotes differentiation with respect to η. Solution is desired in the range $0 \leqslant \eta \leqslant 1$, which is divided into M equal intervals, each of length $\Delta = 1/M$. Equations (17)–(19) are written in the finite-difference form using

$$X_N'=(X_{N+1}-X_{N-1})/2\Delta \quad (20)$$

$$X_N''=(X_{N+1}-2X_N+X_{N-1})/\Delta^2 \quad (21)$$

where X_N stands for any one of the variables at Nth mesh point. To start with, initial guesses are made for all the variables at each of the mesh points, consistent with the boundary conditions. A guess for effective freestream location, n_e, is also made. The variables u_1, v_1 and T_1 are corrected using an acceleration factor which ensures that the correction applied to a variable is never greater in magnitude than ε times the previous value of the variable where ε is a prescribed, small, positive number. The value of n_e is adjusted in each iteration by the requirement that the temperature gradient at the freestream should be small. Full details of SAR method are given in [12].

In each iteration, after correcting u_1, v_1 and T_1 using SAR method, new values of ρ_1 and p_2 are obtained by numerical integration of the first-order equations (10) and (13). Equation (10) gives difficulty in integration at the wall where $v_1 = 0$. To circumvent it, an alternative method is employed here. The density is obtained in the usual way by integrating equation (10) but the integration is carried out only up to one mesh point away from the wall. The corresponding pressures are obtained from the equation of state. The final pressure on the wall is obtained from the linear expression

$$(p_1)_w=(p_1)_\Delta-\Delta(p_1)_w' \quad (22)$$

where $(p_1)_w'$ is obtained from equation (12) by writing it at the first mesh point in finite-difference form.

Knowing $(p_1)_w$, equation of state is used to obtain the density at the wall.

The numerical procedure described above is programmed and the computations are carried out on an IBM 7044 computer. The parameters $\Gamma_0\alpha_0\bar{r}_b$, Re, Pr, γ and M_∞ are prescribed. A finite mesh size of 1/60 is taken. For each set of values, about a thousand iterations are required before proper convergence is achieved, i.e. when the changes in the flow variables occurred only in the fifth or sixth place of decimal.

4. DISCUSSION OF RESULTS

Numerical solutions are obtained for Re varying from 2 to 50 with $M_\infty = 10$, $Pr = 0{\cdot}75$ and $\gamma = 1{\cdot}4$. Radiation parameter $\Gamma_0\alpha_0\bar{r}_b$ is taken as 0, 350 and 700. Under cold wall conditions, $T_w = T_\infty$ is taken but to study the effects of wall temperature variation, $T_w = 0{\cdot}1$ is also considered. A linear μ–T relationship is assumed but $\mu \propto \sqrt{T}$ is also taken to illustrate the effects of different μ–T relationship on the flow characteristics.

In Figs. 2–4, u_1, v_1, T_1, p_1 and ρ_1 profiles are plotted in the stagnation region for $Re = 7{\cdot}0$, $26{\cdot}6$ and $\Gamma_0\alpha_0\bar{r}_b = 0{\cdot}0$, $350{\cdot}0$. It is seen that due to radiation cooling, the temperature level in the merged shock layer is reduced and the merged shock layer becomes thinner. u_1, v_1 and T_1 profiles are compared with the results of Liu and Sogame [3]. Figures 2 and 3 show that these profiles differ considerably from [3] at low Reynolds number while the difference is very little at $Re = 26{\cdot}6$ as is seen from Fig. 4. In the present analysis, the temperature in the merged shock layer is slightly higher, the merged shock layer is thicker

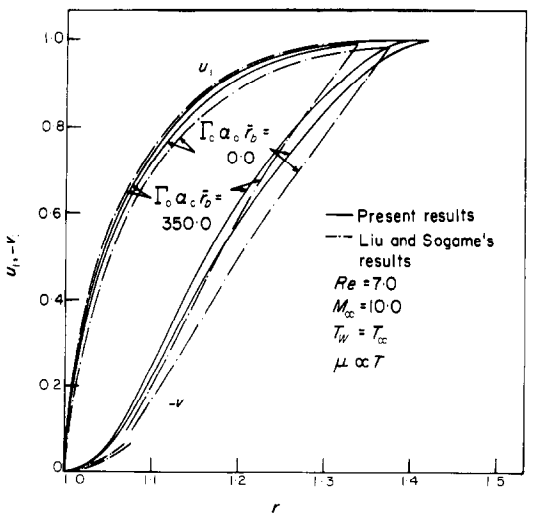

FIG. 2. Tangential and normal velocity profiles in the merged shock layer.

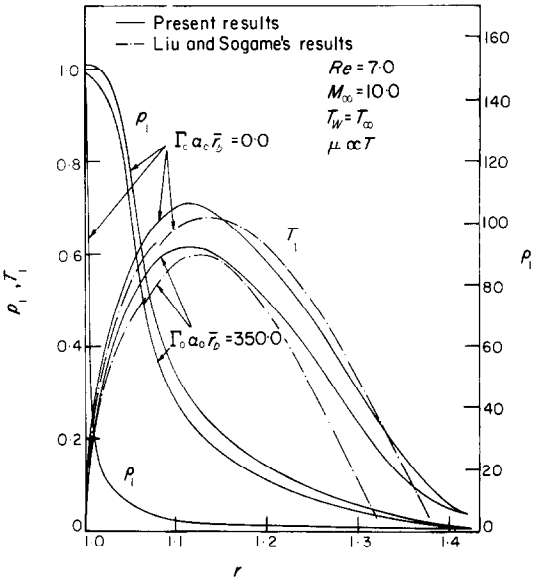

FIG. 3. Temperature, pressure and density profiles in the merged shock layer.

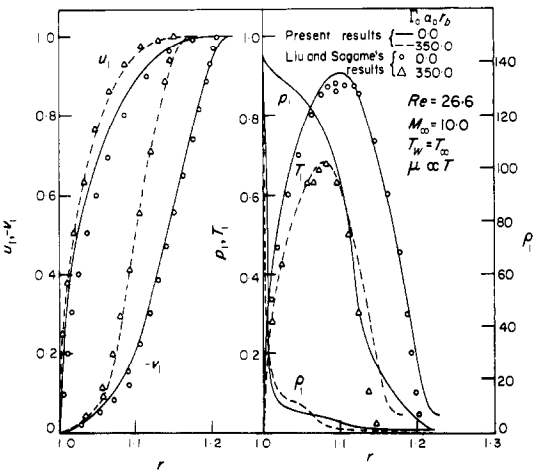

FIG. 4. Velocities, temperature, pressure and density profiles in the merged shock layer.

and the decrease in the thickness due to radiation cooling is not as large as in [3]. The difference at low Reynolds number is due to the fact that the thin-layer assumption is not valid as the thickness of the merged shock layer becomes comparable to the body radius. Since no thin-layer assumption is made here, it is expected that the present results are more reliable at low Reynolds numbers. At moderately high Reynolds number, the merged shock layer is quite thin making the thin-layer assumption valid and so the profiles in the two analysis are very close. Moreover, in the two thin-layer model, there is a discontinuity

in the flow variables at the interface of the two layers due to lack of proper matching. Merging with the freestream is also not smooth. Present analysis removes the discontinuity in the flow variables and the flow smoothly merges with the freestream.

Use of the full Navier–Stokes equations without any assumption on pressure gradient made it possible to calculate the pressure distribution in the stagnation region. Density distribution is also obtained. The effect of radiation cooling on density is insignificant at low Reynolds number but at higher Reynolds number, density first increases near the surface and then decreases from its zero radiation value as shown in Fig. 4.

In Fig. 5, the thickness of the merged shock layer is plotted against Re. The thickness is defined as the distance of the point at which $T_1 = 0{\cdot}1$ from the body surface. It can be seen that at very low Re, the thickness is 0·8–0·9 of the body radius suggesting that the thin-layer approximation is not correct at very low Re. Effect of radiation cooling is to decrease slightly the merged shock layer thickness.

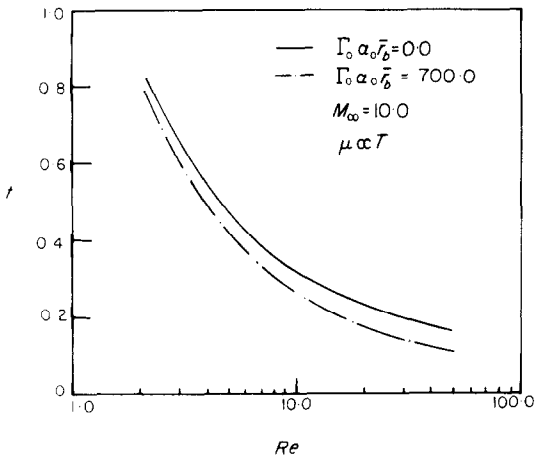

FIG. 5. Merged shock layer thickness vs Reynolds number.

Considering the most important aspect of heat transfer to the body surface by various modes, the local heat transfer rates have been nondimensionalized with respect to $\bar{\rho}_\infty \bar{u}_\infty(\bar{H}_\infty - \bar{H}_w) \simeq \bar{\rho}_\infty \bar{u}_\infty^3/2$ for a cold wall and hypersonic freestream. Convective heat transfer coefficient is given by

$$c_H^c = \frac{\bar{k}_w(\partial \bar{T}/\partial \bar{r})_w}{\bar{\rho}_\infty \bar{u}_\infty^3/2} = \frac{2A\mu_w}{Pr\ Re\ n_e}\left(\frac{\partial T}{\partial \eta}\right)_w. \qquad (23)$$

The contribution from the radiative heat flux to the surface is obtained by the following integral

$$\bar{q}_w^R = \tfrac{1}{2}\int_{\bar{r}_b}^{\infty} \bar{\rho}\kappa 4\sigma \bar{T}^4\, d\bar{r} = 2\sigma \int_{\bar{r}_b}^{\infty} C\bar{\rho}\bar{T}^8\, d\bar{r}.$$

In terms of heat transfer coefficient, radiative heat transfer coefficient is given by

$$c_H^R = \bar{q}_w^R/(\bar{\rho}_\infty \bar{u}_\infty^3/2) = n_e A(\Gamma_0\alpha_0\bar{r}_b)\int_0^1 pT^8\, d\eta. \qquad (24)$$

The total heat transfer coefficient c_H^{R+c} can be obtained by adding (23) and (24).

In Fig. 6, c_H^c, c_H^R and c_H^{R+c} are plotted against Re for $\Gamma_0\alpha_0\bar{r}_b = 700$. c_H^0 curve is for zero radiation case i.e. when $\Gamma_0\alpha_0\bar{r}_b = 0$. It is seen that the radiation cooling reduces the convective heat transfer to the surface.

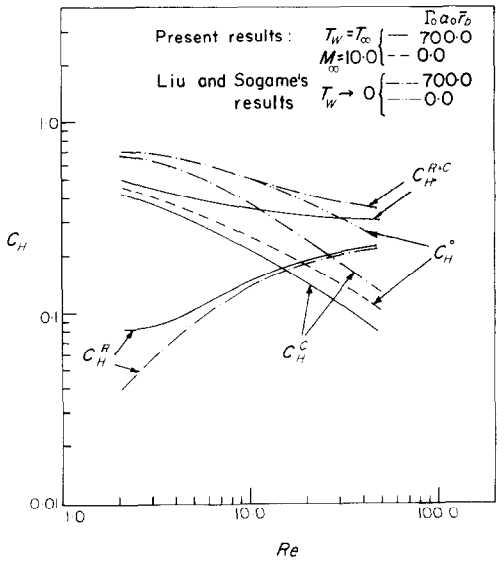

FIG. 6. Convective, radiative and total heat transfer vs Reynolds number.

Further, c_H^R decreases with decrease in Re while c_H^c increases. Results are compared with that of Liu and Sogame [3]. Present analysis gives slightly higher values of c_H^R and the difference decreases as the Reynolds number increases. The difference in c_H^c curve seems to be mainly due to the wall temperature effect. In the present work, when the wall temperature was changed from $T_w = T_\infty = 0{\cdot}0476$ to $T_w = 0{\cdot}1$ to see the effect of wall temperature, it was found that the c_H^c curve moved considerably towards the curve of Liu and Sogame while c_H^R curve was hardly affected. This is explained from Fig. 7 which shows that changing the wall temperature from 0·0476 to 0·1 does not affect the various profiles except that the surface density is decreased. Since c_H^R is an integrated effect of

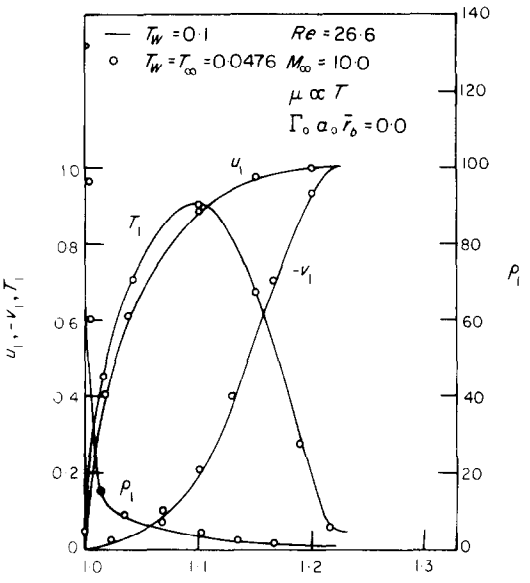

FIG. 7. Effect of wall temperature variation.

temperature distribution in the merged shock layer which is not altered due to the change in wall temperature from 0·0476 to 0·1, c_H^R curve remains practically unchanged.

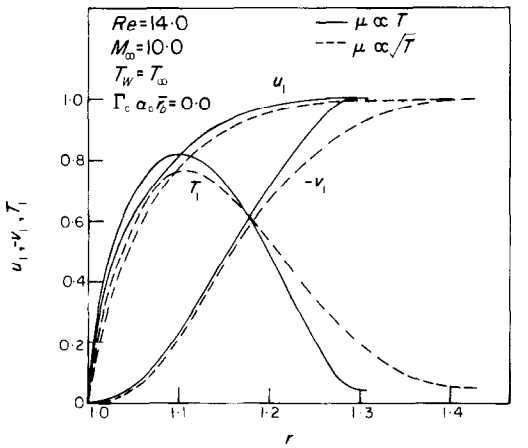

FIG. 8. Effect of μ–T relationship.

In the end, to see the effect of μ–T relationship, u_1, v_1 and T_1 curves are plotted in Fig. 8 for $\mu \propto T$ and for $\mu \propto \sqrt{T}$. Only zero radiation case is considered. It is seen from Fig. 8 that the merged shock layer thickness is increased when $\mu \propto \sqrt{T}$ since it effectively decreases the value of Reynolds number.

REFERENCES

1. H. K. Cheng, Viscous hypersonic blunt-body problems and the Newtonian theory, *International Symposium on Fundamental Phenomenon in Hypersonic Flow*, edited by J. Gordon Hall, pp. 90–131 (1965).
2. A. C. Jain, Hypersonic flow at low Reynolds number near the stagnation point of a blunt-body, *Proceedings of Summer Seminar on Fluid Mechanics*, edited by P. L. Bhatnagar, pp. 65–80. I.I.Sc., Bangalore, India (1967).
3. J. T. C. Liu and E. Sogame, Radiative transfer in the low Reynolds number, blunt-body stagnation region at hypersonic speeds, *AIAA Jl* (7), 1273 (1969).
4. H. K. Cheng, Hypersonic shock layer theory of the stagnation region at low Reynolds number, *Proceedings of the 1961 Heat Transfer and Fluid Mechanics Institute*, pp. 161–175. Stanford University Press, Calif. (1961).
5. H. K. Cheng, The blunt-body problem in hypersonic flow at low Reynolds number, Rept. AF 1285-A-10, Cornell Aeronatucal Laboratory, Buffalo, N.Y. (1963).
6. V. Adimurthy and A. C. Jain, Hypersonic rarefied flow near the stagnation region of a blunt body, Accepted for presentation at the 8th International Symposium on Rarefied Gas Dynamics held at Stanford, Calif., 10–14 July (1972).
7. J. T. Howe and J. R. Viegas, Solutions of the ionized radiating shock layer including reabsorption and foreign species effects and stagnation region heat transfer, NASA TR R-159 (1963).
8. O. R. Burggraf, Asymptotic solution for the viscous radiating shock layer, *AIAA Jl* (10), 1725 (1966).
9. H. Hoshizaki and K. H. Wilson, Viscous radiating shock layer about a blunt-body, *AIAA Jl* (9), 1614 (1965).
10. H. Hoshizaki and K. H. Wilson, Convective and radiative heat transfer during superorbital entry, *AIAA Jl* (1), 25 (1967).
11. S. C. Traugott, A differential approximation for radiative transfer with application to normal shock structure, *Proceedings of the 1963 Heat Transfer and Fluid Mechanics Institute*, pp. 1–13. Stanford University Press, Stanford, Calif. (1963).
12. T. C. Dellinger, Computation of nonequilibrium merged stagnation shock layers by successive accelerated replacement, *AIAA Jl* (2), 262 (1971).

COUCHE DE CHOC HYPERSONIQUE ET RAYONNANTE, PROCHE DE LA REGION D'ARRET D'UN CORPS ÉMOUSSÉ

Résumé—Dans un écoulement à nombre de Reynolds modéré, l'onde de choc et la couche visqueuse proches du point d'arrêt d'un corps émoussé sont fondues ensemble. Cette couche de choc est étudiée ici pour un gaz rayonnant. Le transfert par rayonnement est simplifié. Le modèle d'écoulement est décrit par les équations complètes de Navier–Stokes. En utilisant le concept de similarité locale, les équations sont réduites à un système d'équations différentielles non linéaires, couplées, du huitième ordre. Ce système d'équations est intégré numériquement entre la surface et l'écoulement libre sous différentes conditions de pression.

Auparavant ce problème avait été étudié par Lin et Sogame [3] dans le cadre d'un modèle à deux couches minces. On a dégagé un certain nombre d'inexactitudes dans cette analyse. On montre que la présente étude donne une information plus précise sur le comportement détaillé de l'écoulement visqueux émissif aux nombres de Reynolds modérés.

HYPERSONISCHE STOSSSCHICHT MIT STRAHLUNG IN DER STAUZONE EINES STUMPFEN KÖRPERS

Zusammenfassung—Bei niedrigen Reynolds-Zahlen verschmelzen Stossschicht und viskose Schicht in der Nähe des Staupunkts eines stumpfen Körpers miteinander. Diese verschmolzene Stossschicht wird in dieser Arbeit an einem strahlenden Gas untersucht. Die Strahlung wird auf den Fall überwiegender Emission beschränkt. Mit Hilfe der lokalen Ähnlichkeit werden die Gleichungen reduziert auf einen Satz von nichtlinearen, gekoppelten, gewöhnlichen Differentialgleichungen achter Ordnung. Dieser Gleichungssatz wird numerisch integriert von der Fläche bis zur freien Strömung unter verschiedenen Bedingungen. Vorher wurde das Problem von Liu und Sogame [3] mit Hilfe eines Modells mit zwei dünnen Schichten behandelt. Ungenauigkeiten dieser analytischen Entwicklung werden aufgezeigt. Die vorliegende Analyse gibt eine zuverlässigere und genauere Information über das besondere Verhalten der viskosen Strömung mit Strahlung bei niedrigen Reynolds-Zahlen.

ГИПЕРЗВУКОВОЙ ИЗЛУЧАЮЩИЙ СЛИТЫЙ УДАРНЫЙ СЛОЙ В ОКРЕСТНОСТИ КРИТИЧЕСКОЙ ТОЧКИ ЗАТУПЛЕННОГО ТЕЛА

Аннотация—При течении с малым числом Рейнольдса ударнар волна и вязкий слой сливаются в окрестности критической точки затупленного тела. В настоящей работе такой слитый ударный слой исследуется в излучающем газе. Лучистый перенос упрощается и сводится к случаю доминирующей эмиссии. Основная модель потока описывается полными уравнениями Навье-Стокса. Используя понятие локального подобия, уравнения сводятся к нелинейным сдвоенным обычным дифференциальным уравнениям восьмого порядка. Ранее эта задача исследовалась Лиу и Согеймом [3] на модели двух тонких слоев. Указывается на ряд неточностей этой аналитической разработки. Показано, что данный анализ дает более надежные и точные сведения о поведении лучистого вязкого потока при малом числе Рейнольдса.